Compositional Engineering for Efficient Wide Band Gap Perovskites with Improved Stability to Photoinduced Phase Segregation

Kevin A. Bush[1], Kyle Frohna[1,2], Rohit Prasanna[1], Rachel E. Beal[1], Tomas Leijtens[1], Simon A. Swifter[1], Michael D. McGehee[1]
[1]*Materials Science & Engineering, Stanford University, Stanford, 94305, USA.*
[2]*School of Physics, Trinity College Dublin, Dublin 2, Ireland.*
Mmcgehee@stanford.edu

Abstract:

Metal halide perovskites are attractive candidates for the wide band gap absorber in tandem solar cells. While their band gap can be tuned by partial halide substitution, mixed halide perovskites often have lower open circuit voltage than would be expected and experience photoinduced trap formation caused by halide segregation. We investigate solar cell performance and photostability across a compositional space of formamidinium (FA) and cesium (Cs) at the A-site at various halide compositions, and show that using more Cs at the A-site rather than more Br at the X-site to raise band gap is more ideal as it improves both V_{OC} and photostability. We develop band gap maps and design criteria for the selection of perovskite compositions within the $Cs_xFA_{1-x}Pb(Br_yI_{1-y})_3$, space. With this we identify perovskites with tandem-relevant band gaps of 1.68 and 1.75 eV that demonstrate high device efficiencies of 17.4 and 16.3%, respectively, and significantly improved photostability compared to the higher Br containing compositions.

Silicon solar cells currently own 93% of the solar market as costs have plummeted, outpacing even Swanson's law which estimates that the cost of photovoltaics will drop 20% for every doubling of cumulative volume sold[1]. This rapid cost reduction caused problems to a growing CIGS industry, whose promise of inexpensive thin film manufacturing at a comparable efficiency to silicon has still yet to be fully realized. Metal-halide perovskites, with the formula ABX_3 (A = methylammonium (MA), formamidinium (FA), Cs, B = Pb, Sn, and X = I, Br) are rapidly gaining attention for thin film photovoltaics, due to their long carrier diffusion lengths[2], defect tolerance enabling versatile solution or vapour processing[3,4], and strong optical absorption[5]. Rather than challenging the incumbent silicon, the wide, tunable band gap of perovskites holds the promise of boosting the efficiency of silicon by employing them as the wide-gap absorber in tandem solar cells on silicon, which offer a path to surpassing fundamental efficiency limits on single-junction solar cells[6] by extracting a portion of photo-generated carriers at a higher voltage[7–14]. Perovskite-silicon tandems have recently achieved record efficiencies of 23.6% for monolithically integrated[15] and 26.4% for mechanically stacked configurations[16]. Additionally, recent developments in the stability and efficiency of low band gap tin-based perovskites have drawn attention for making highly efficient and potentially low cost perovskite-perovskite tandems[17,18].

A major benefit of perovskites for top cells in tandems is the ability to continuously raise the band gap, which was first done by substituting bromide for iodide. Noh et al demonstrated that given the general composition $MAPb(Br_xI_{1-x})_3$, where MA is methylammonium, the band gap can be continuously tuned between 1.5 and 2.3eV simply by varying x[19]. However, thus far, open circuit voltages have not increased linearly with increasing band gap upon Br substitution[20], negating part of the benefit of using a tandem configuration. The disappointing voltages are likely a consequence of higher trap densities or traps deeper within the band gap in bromine-rich perovskites[21]. In some cases it is clear that

photoinduced halide segregation, referred to here as the Hoke effect[22], occurs. Upon illumination, segregation of the halides into lower band gap I-rich and higher band gap Br-rich regions, mediated by halogen vacancies[23,24], occurs on the timescale of seconds for the pure MA-based perovskites. Photo-generated carriers are funneled towards these lower band gap regions, which act as recombination centers, resulting in a loss in voltage[25,26].

Substitution and alloying on the A-site by replacing MA with Cs and Formamidinium (FA) has led to record efficiencies[27,28] and improved structural, thermal, and moisture stability of perovskites[29–31]. Further, while targeting band gaps of approximately 1.73eV for tandems, McMeekin et al demonstrated improved photo-stability (reduced halide phase segregation) with 40% Br, albeit under milder illumination conditions than those experienced under AM1.5G[32]. Duong et al took this a step further and employed four cations, Rb, Cs, FA, and MA, for improved maximum power stability with 33% Br[33]. Both of the studies reported stability against phase separation at less than one-sun illumination and neither composition achieves photo-stability at one-sun equivalent intensity. Our group has previously demonstrated how using only Cs on the A-site prevents halide phase segregation with up to 33% Br incorporation[34], but the 1.9eV band gap and low efficiency limits its efficacy in tandems.

In this work, we characterize the FA/Cs and I/Br compositional space and develop design rules for targeting band gaps of 1.68 and 1.75 eV due to their relevance for tandems. We find that higher open circuit voltages are achieved and photostability is improved when the band gap is attained by raising the Cs fraction more than the Br fraction. We fabricate devices using two perovskite compositions for each band gap: a high Cs, low Br composition, and a low Cs, high Br composition. We find the 1.68 eV band gap devices behave similarly, whereas for the 1.75 eV band gap devices, higher Cs, lower Br compositions yield higher performances due to increased voltage and fill factor (FF). Finally, we demonstrate significantly improved photoluminescence (PL) stability at one-sun equivalent laser illumination in perovskite compositions with tandem-relevant band gaps enabled by using higher Cs and lower Br contents.

FA/Cs and I/Br Compositional Space for Band Gap Tuning

Although the A-site cation does not contribute to the density of states at the band-edge, it can tune the band gap by changing the crystal structure[35], as shown computationally[36,37] and experimentally[38]. Using a smaller cation, such as Cs, can tilt the BX_6 octahedra when in the tetragonal structure, reducing the X-B-X bond angle and increasing band gap[39]. Thus, tuning the A-site cation composition can reduce reliance on Br to achieve wide band gaps for tandem top cells.

We fabricate films and solar cells using perovskites with the composition $Cs_xFA_{1-x}Pb(Br_yI_{1-y})_3$, where we systematically vary x from 15 to 40% and y from 5 to 30%. The Cs/FA composition ratio was varied by changing the relative concentrations of CsI and FAI and the Br/I composition ratio was varied by changing the relative concentrations of $PbBr_2$ to PbI_2 in the precursor solution. 1M solutions were dissolved in DMF and DMSO at a ratio of 4:1. The four precursor salts were weighed out and added to the same vial prior to adding solvent. Both devices and films of 30 different perovskite compositions were fabricated. All single junction perovskite devices were fabricated in the p-i-n architecture. Briefly, 5 mg/mL PTAA in chlorobenzene was spun on top of ITO-coated glass to act as the hole selective contact, as it has been shown to enable high V_{OC} p-i-n architecture solar cells[40,41]. A modified version of the compressed air gas quenching (CAGQ) method was used to fabricate the perovskite layers[42]. The CAGQ method was preferred over the popular antisolvent route[43] to avoid

dissolution of the organic PTAA layer. Additionally, we found the CAGQ method to be easily adaptable to a wide variety of compositions. The devices were finished with evaporated C60, BCP, and Ag. Further details on the fabrication procedure can be found in the experimental section.

Figures 1B-E show how for Br contents between 11.25 and 30% the perovskite band-edge smoothly blue shifts with increasing Cs content, based on EQE. A high current density can be extracted from nearly all perovskite compositions studied, as seen in the integrated photocurrent from EQE in Figure 1F, indicating that the CAGQ method enabled the fabrication of high quality film perovskite films across the wide compositional space. Poorer performance, in terms of both low EQE and V_{OC}, was consistently observed for compositions with a large fraction of Cs and 5% Br (Figure 1A). The champion measured performance for these compositions is plotted. Film formation in this high Cs, low Br region was considerably slower than in other areas of the phase space and XRD of the Cs40Br5 composition displays several non-perovskite peaks (Figure S1E). Thus, the poor performance of the high Cs, low Br compositions is likely a result of this poor phase purity. XRD was also measured for low Cs compositions and for high Cs, high Br compositions and only the perovskite peaks are observed (Figure S1), indicating a higher degree of phase purity in the rest of the compositional space.

Figure 1G shows the band gap as a function of composition, determined from Tauc plots of absorption spectra. To quantify the capability of Cs and Br to tune the band gap, we fit the variation in band gap versus composition with a linear function and extracted the slope. We found a cesium band gap coefficient of 2.3 ± 0.2 meV/% Cs and a bromine band gap coefficient of 5.7 ± 0.2 meV/% Br for this phase space, showing that an increase in Cs content produces slightly less than half of the band gap change produced by an equivalent increase in Br content.

Figure 1H shows the best open circuit voltage (V_{OC}) attained from devices of each perovskite composition. Promisingly, we find that increasing Cs content at a fixed I/Br ratio does result in an increase in V_{OC} alongside the increasing band gap. We have plotted the band gap and V_{OC} maps (Figures 1G and 1H) side by side with a proportionate y axis scale for direct comparison. We observe that the lines have roughly the same slope, indicating that with increasing band gap upon Cs substitution in eV, the V_{OC} rises a nearly equivalent amount in q*V (barring the high Cs, low Br compositions). In contrast, the wide spacing between the separate lines, indicative of a large increase in band gap with more Br, does not match with the relatively narrow separation between lines in the V_{OC} plot. This shows that while raising Br content is effective at raising the band gap, it fails to realize equivalent rises in the V_{OC}. This V_{OC} plateau, observed upon increasing the band gap by tuning the I/Br ratio, has been observed previously in both the p-i-n and n-i-p architectures[44–46]. Using Cs at the A-site instead of Br at the X-site to raise the band gap is effective for both realizing higher band gap and equivalently higher V_{OC}.

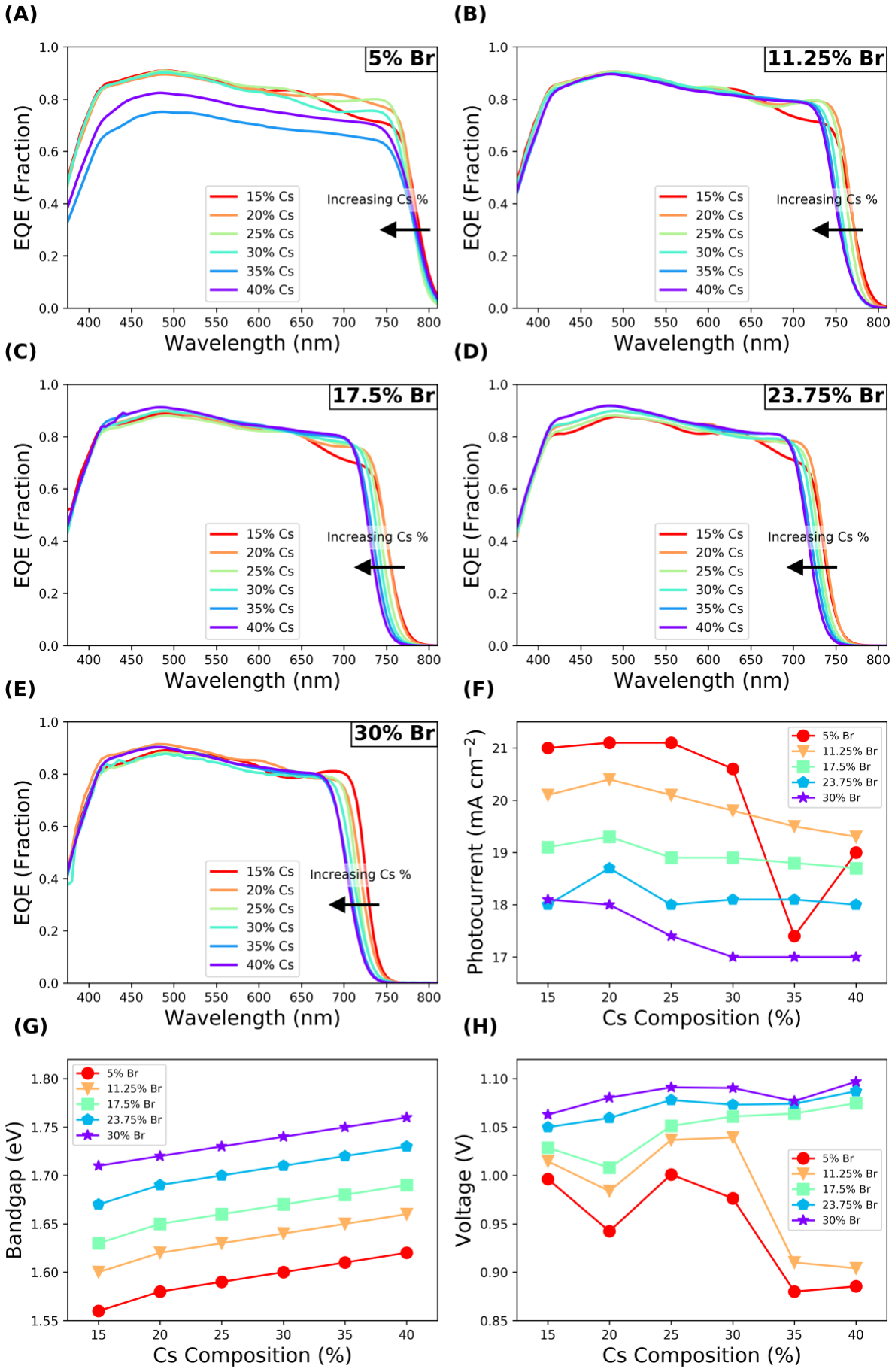
(A)
5% Br
(B)
11.25% Br
(C)
17.5% Br
(D)
23.75% Br
(E)
30% Br
EQE (Fraction)
Wavelength (nm)
15% Cs
20% Cs
25% Cs
30% Cs
35% Cs
40% Cs
Increasing Cs %
(F)
Photocurrent (mA cm^{-2})
Cs Composition (%)
5% Br
11.25% Br
17.5% Br
23.75% Br
30% Br
(G)
Bandgap (eV)
(H)
Voltage (V)

Figure 1: (A), (B), (C), (D), and (E) EQE for 5, 11.25, 17.5, 23.75, and 30% Br content, respectively, showing how increasing Cs causes the band edge to blue shift, (F) integrated photocurrent density from EQEs in Figures 1a-e, (G) band gap, and (H) V_{OC} vs perovskite composition for the $Cs_xFA_{1-x}Pb(Br_yI_{1-y})_3$ compositional space, showing change in Cs along the x axis and change in Br from 5 to 30% as separate lines. Note, band gap values are calculated from Tauc plots based on absorption and V_{OC} is plotted based on the champion device from one perovskite device batch to mitigate day-to-day batch variations.

The map of band gaps across compositional space enables us to evaluate different compositions that have the same band gap to compare performance and photo-stability. We hone in on two band gaps: 1.75 eV, corresponding to the Shockley Quiesser ideal top cell band gap on silicon[47] and use in realistic all-perovskite tandems[48,49], and 1.68 eV, corresponding to the band gap that Hörantner and Snaith found to maximize efficiency and energy yield for perovskite/silicon tandems under real world conditions taking into account the fact that the perovskite cell does not absorb all of the light right at the band edge. For brevity, we refer to perovskite compositions based on their Cs and Br contents. For example, $Cs_{0.17}FA_{0.83}Pb(Br_{0.25}I_{0.75})_3$ will be referred to as Cs17/Br25.

For 1.68 eV band gap perovskites, we study the Cs17/Br25 and Cs25/Br20 compositions. Both compositions make efficient solar cells – notably, the Cs25/Br20 perovskite reaches over 17 %, with higher FF than the Cs17/Br25 (Figure 2A, B). For perovskites with 1.75 eV band gaps, we focus on Cs17/Br40 and Cs40/Br30 compositions. The Cs40/Br30 composition also displayed a high efficiency of 16.3 % with a V_{OC} of 1.17 V (Figure 2). The V_{OC}s are slightly higher than in Figure 1 because Figure 2 shows our champion device performance, while Figure 1 shows data all from the same batch of devices for consistency. However, the wide band gap Cs17/Br40 composition shows a lower V_{OC} and performance than the Cs40/Br30 composition. We suspect that the higher bromine contents needed to reach the larger band gaps introduce either an increased concentration of non-radiative recombination sites or makes those sites deeper in energy relative to the relevant band[21,50], which can be avoided by instead increasing band gap through Cs substitution. Additionally, time resolved photoluminescence (TRPL) measurements (Figure S2) show that for each targeted band gap, the lifetime of the high Cs, low Br composition is longer than that of the low Cs, high Br composition. Lifetime and J-V performance parameters for the four compositions of interest are provided in Table 1 for comparison. The significantly higher FF for Cs25/Br20 composition is likely related to it having a longer PL lifetime than the Cs17/Br25 composition. These results suggest that the strategy of raising the band gap through Cs composition becomes increasingly important at higher band gaps relevant for tandems. An open-circuit voltage of 1.17 V and efficiency of 16.3 % is comparable to the highest reported for perovskites solar cells with band gaps between 1.7-1.8eV in the inverted p-i-n architecture[44,51], and was achieved using no additional defect passivation. Higher voltages for mixed halide perovskites have been obtained in the n-i-p architecture[32,45,46,52,53]; however, an analysis of what is limiting the voltage of the p-i-n architecture is beyond the scope of this work. To emphasize the utility of the FA/Cs and Br/I compositional space map, we also fabricated another 1.68 eV band gap perovskite with the Cs35/Br18 composition. The similarly high device efficiency of 17.3 % with a V_{OC} of 1.12 V, as illustrated in the JV and EQE data in Figure S3, speaks to the efficacy of the higher Cs containing perovskite compositions.

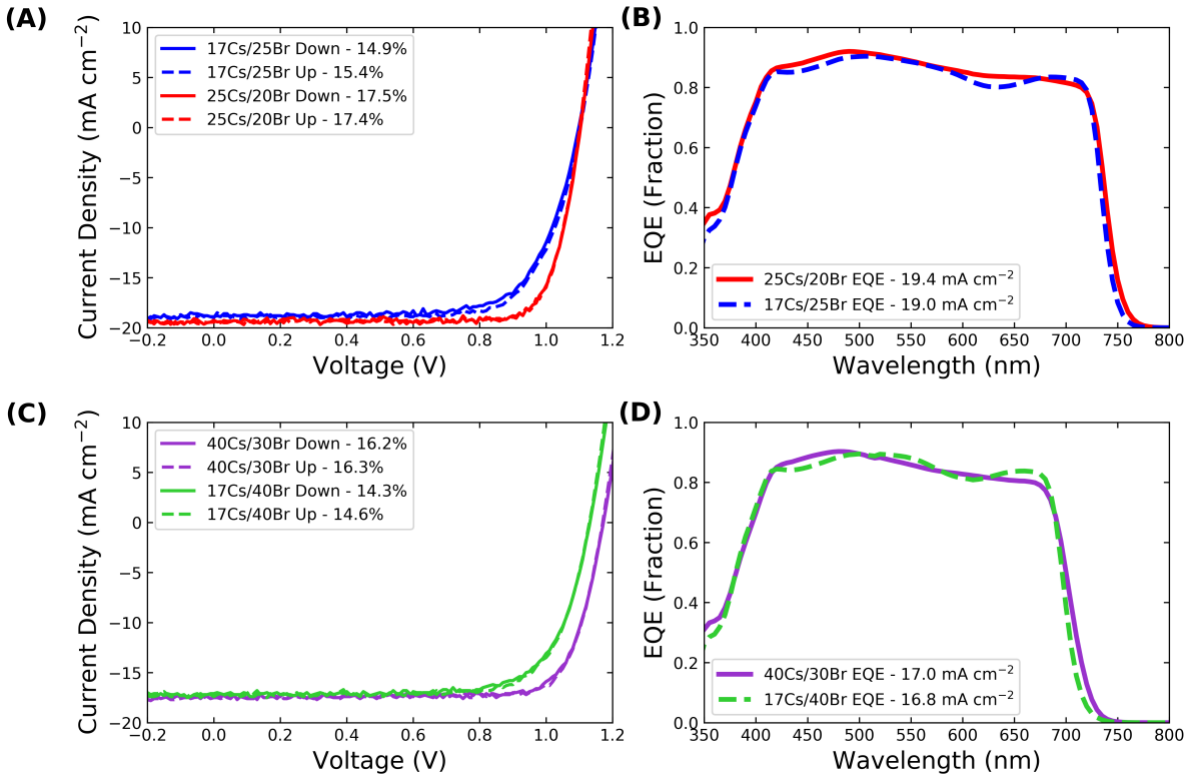

Figure 2. JV (A and C) and EQE (B and D) plots of the 1.68eV (A and B) and 1.75eV (C and D) band gap perovskites displaying the high performance of the high Cs containing compositions.

Compositions	τ (ns)	V_{OC} (V) Up/Down	J_{SC} (mA cm^{-2}) Up/Down	FF Up/Down	PCE (%) Up/Down
17Cs/25Br	6	1.10/1.10	19.0/18.9	0.74/0.72	15.4/14.9
25Cs/20Br	50	1.10/1.10	19.4/19.3	0.81/0.82	17.4/17.5
17Cs/40Br	6	1.13/1.13	17.4/17.1	0.74/0.74	14.6/14.3
40Cs/30Br	12	1.17/1.17	17.5/17.5	0.8/0.79	16.3/16.2

Table 1. TRPL lifetimes extracted from Figure S2 and performance parameters from Figure 2 for the different perovskite compositions.

Hoke Effect Studies on 1.68 and 1.75eV Band Gap Perovskites

A benefit of raising band gap with Cs is that the same band gap can be achieved with a lower concentration of Br. This increases photostability, as higher Br contents lead to more rapid halide segregation under illumination (the Hoke effect)[22,34]. To compare the susceptibility of the 1.68 and 1.75 eV band gap perovskite compositions to the Hoke effect, we measured PL vs illumination time over a range of illumination intensities on devices of all four compositions. A continuous wave, 488 nm wavelength laser was used for excitation. To calibrate the illumination intensity, the laser power was tuned to reach the same current density as under simulated 1-sun illumination. We note that we have calibrated the illumination intensity rather than carrier density, which is likely to be far lower in these devices compared to films due to additional nonradiative recombination pathways related to interfaces with the contacts used. A red-shift in the PL peak over time or a lower energy peak forming is indicative of lower-band gap, I-rich trap states forming, as seen by Hoke et al[22]. At 0.1 suns, the Cs17/Br25 composition begins to show a low energy PL peak growing over the course of 10 minutes and at 1 sun this peak becomes more obvious (Figure 4A). In contrast,

the Cs25/Br20 composition shows almost no lower energy peak forming at 1 sun over the course of 10 minutes (Figure 3B). At 10 suns, the Hoke effect clearly occurs in the Cs17/Br25 perovskite, as a large peak forms around 775 nm. No such peak is apparent in the Cs25/Br20 composition even at 10 suns highlighting good photostability of the high-Cs low-Br composition.

The 1.75 eV band gap compositions, Cs17/Br40 and Cs40/Br30, show a far more striking difference in the PL stability (Figure 3C, D). Previous reports of perovskite devices with a ~1.75 eV band gap have either suffered from poor photo-stability at intensities approaching 1 sun or lower power conversion efficiency[17]. The Cs17/Br40 perovskite shows the Hoke effect at as little as 0.03 suns in 10 minutes, whereas the Cs40/Br30 shows only a slight shift at 10 suns over 10 minutes, in Figure 3C and 3D. As suggested in the previous section, band gap tuning with Cs becomes even more important at higher band gaps as one can mitigate a large voltage loss and increase photostability simultaneously.

We also monitor V_{OC} during each PL measurement (Figure 4) and see that phase segregation is correlated with a loss in V_{OC}. The high Cs, low Br compositions have a more stable V_{OC} under laser illumination than low-Cs compositions with the same band gaps. Most notable is the significantly improved V_{OC} stability at 10 suns for the high Cs compositions. However, even samples that do not undergo an obvious change in PL emission still lose V_{OC} (Figure 4). This could be due to small amounts of halide segregation, undetectable in our PL measurements, that would cause recombination through lower band gap I-rich trap states, resulting in V_{OC} loss. To reinforce this point, the evolution of the PL center of mass in energy is compared to the V_{OC} loss over time in Figure S5, for each composition. It is apparent that the change in PL center of mass follows a similar trend to the loss in V_{OC}. Thus, Figure 4 also suggests that V_{OC} stability alone is a fairly good proxy for stability to halide segregation and is potentially more important and relevant to monitor.

At 1 sun intensity, the Cs17/Br25 and Cs25/Br20 drop 14 and 5 mV, respectively, and the Cs17/Br40 and Cs40/Br30 compositions drop 23 and 7 mV, respectively, over 10 minutes. This highlights that while stability to halide segregation has been improved, increasing Cs and lowering Br does not stop the Hoke effect from occurring, it just suppresses the rate at which it occurs. It is important to note that we fabricate perovskite films using the CAGQ method which produces smaller grains (Figure S6) than those fabricated by McMeekin et al, and a smaller number of grain boundaries can lead to a suppression of halide segregation[51]. This suggests that these compositions could be made more stable yet with optimized deposition conditions.

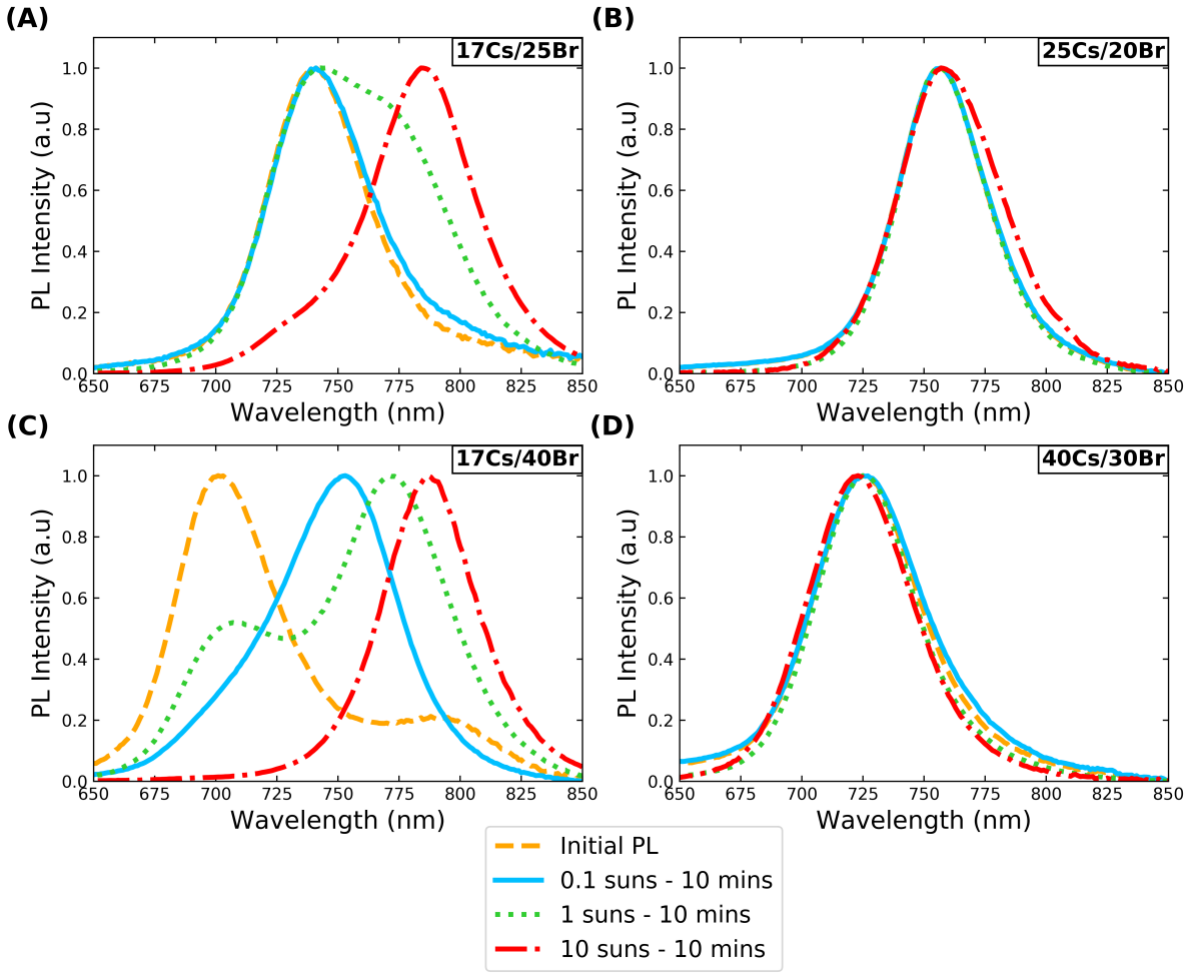

Figure 3. Device PL data comparing Cs17/Br25 and Cs25/Br20 perovskites with a 1.68eV band gap (panels A and B) and Cs17/Br40 and Cs40/Br30 perovskites with a roughly 1.75eV band gap (panels C and D). The initial PL peak is shown as the orange dashed curve. The final PL peaks after 0.1, 1 and 10 suns of excitation for 10 minutes with a 488nm laser are shown for each composition. Devices were held at open circuit during the measurement.

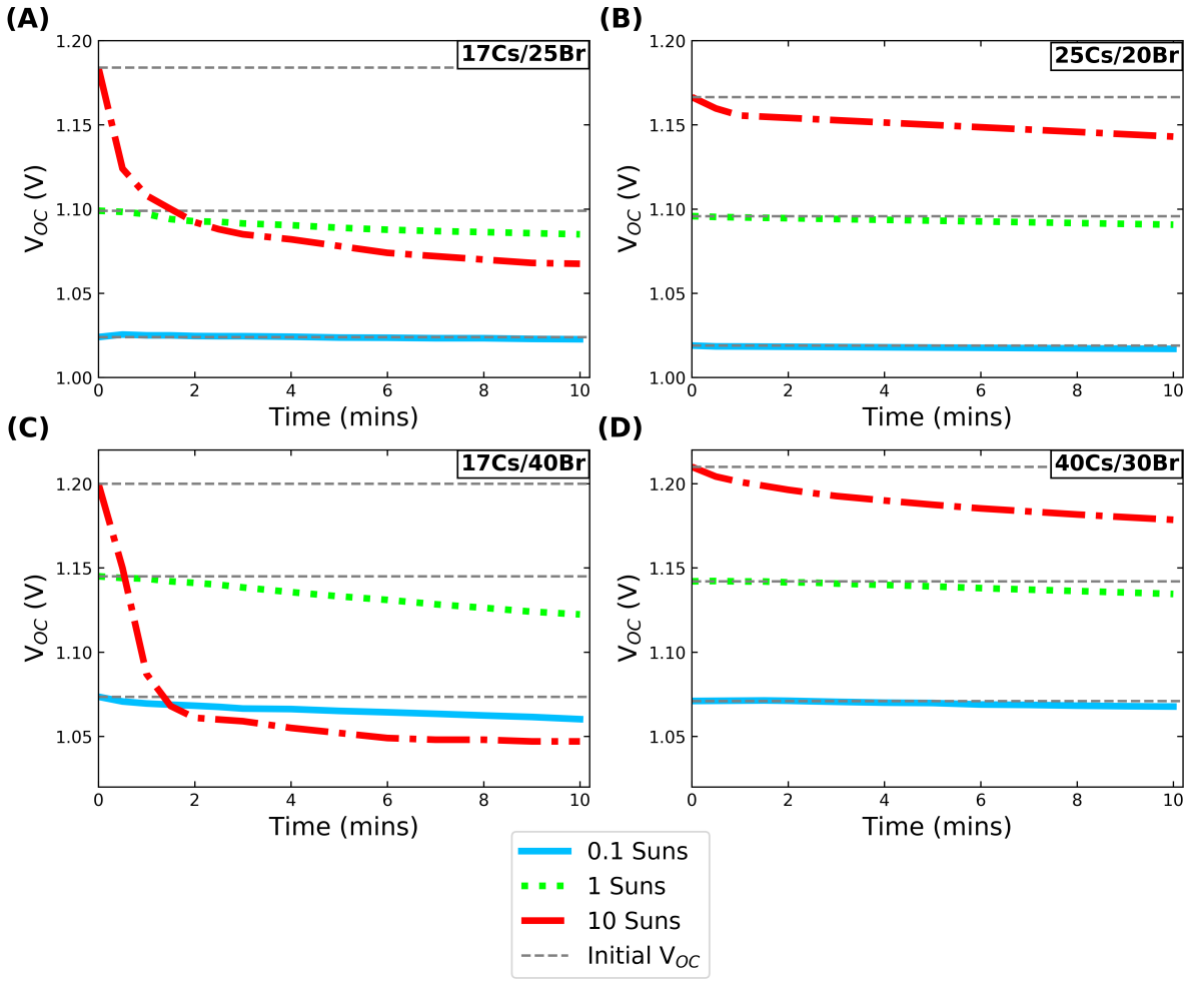

Figure 4. Open-circuit voltage monitored during the PL measurements in Figure 3 at 0.1, 1, and 10 suns comparing Cs17/Br25 and Cs25/Br20 perovskites with a 1.68eV band gap (panels A and B) and Cs17/Br40 and Cs40/Br30 perovskites with a roughly 1.75eV band gap (panels C and D).

Following on previous success in A-site compositional engineering, we have explored the $Cs_xFA_{1-x}Pb(Br_yI_{1-y})_3$ space with the goal of finding compositions that show both high efficiency and improved photo-stability with band gaps suitable to achieve efficient tandems. Increasing band gap with Cs reduces reliance on Br to realize high performance wide band gap perovskites with suppressed halide segregation. Through our exploration of the FA/Cs and I/Br compositional space we have found that low Br and high Cs leads to reduced V_{OC} and EQE, while high Br and low Cs result in poorer stability to halide segregation and an unstable V_{OC}. Thus, as a rule of thumb, we believe it is desirable to have slightly more Cs than Br, percentage-wise, in a wide band gap perovskite composition, with Cs25/Br20 and Cs40/Br30 arising as our champion compositions for 1.68 and 1.75 eV band gaps, respectively. Combining this approach with others reported in the literature, such as obtaining greater control of defect density and grain size during film formation and lowering ionic mobility through quasi-2D structures[45,52] in these higher Cs-containing, mixed halide compounds present a pathway to further suppressing halide segregation and improve the photo-stability to thousands of hours. It remains to be seen whether photo-induced phase segregation can be suppressed to the point of attaining 25-year operational lifetimes with band gaps in excess

of 1.7 eV, but increased Cs concentration and compositional engineering bring that goal one step closer.

Acknowledgments:
The information, data, or work presented herein was funded in part by the U.S. Department of Energy (DOE) Sunshot PVRD2 program under award number DE-EE0008167 and the National Science Foundation (NSF) and Department of Energy under NSF Cooperative Agreement No. EEC-1041895. K.A.B. is supported by the NSF Graduate Research Fellowship Program under Grant No. DGE-114747. TL is funded by a Marie Sklodowska Curie International Fellowship under grant agreement H2O2IF-GA-2015-659225.

Supporting Information Available: Perovskite device fabrication details, J-V measurements, optical measurements, and supplementary figures 1-6.

References.

(1) Fraunhofer ISE. *Photovoltaics Report, Updated: 12 July 2017*.

(2) Stranks, S. D., Stranks, S. D., Eperon, G. E., Grancini, G., Menelaou, C., Alcocer, M. J. P., Leijtens, T., Herz, L. M., Petrozza, A., Snaith, H. J. Electron-Hole Diffusion Lengths Exceeding 1 Micrometer in an Organometal Trihalide Perovskite Absorber. *Science*. **2014**, *342*, 341–344.

(3) Brandt, R. E., Stevanović, V., Ginley, D. S., Buonassisi, T. Identifying Defect-Tolerant Semiconductors with High Minority Carrier Lifetimes: Beyond Hybrid Lead Halide Perovskites. *MRS Commun.* **2015**, *5*, 265–275.

(4) Steirer, K. X., Schulz, P., Teeter, G., Stevanovic, V., Yang, M., Zhu, K., Berry, J. J. Defect Tolerance in Methylammonium Lead Triiodide Perovskite. *ACS Energy Lett.* **2016**, *1*, 360–366.

(5) Green, M. a., Ho-Baillie, A., Snaith, H. J. The Emergence of Perovskite Solar Cells. *Nat. Photonics*. **2014**, *8*, 506–514.

(6) Shockley, W., Queisser, H. J. Detailed Balance Limit of Efficiency of P-N Junction Solar Cells. *J. Appl. Phys.* **1961**, *32*, 510–519.

(7) Bailie, C. D., Christoforo, M. G., Mailoa, J. P., Bowring, A. R., Unger, E. L., Nguyen, W. H., Burschka, J., Pellet, N., Lee, J. Z., Grätzel, M., *et al.* Semi-Transparent Perovskite Solar Cells for Tandems with Silicon and CIGS. *Energy Environ. Sci.* **2014**, *8*, 956–963.

(8) Bailie, C. D., McGehee, M. D. High-Efficiency Tandem Perovskite Solar Cells. *MRS Bull.* **2015**, *40*, 681–686.

(9) Mailoa, J. P., Bailie, C. D., Johlin, E. C., Hoke, E. T., Akey, A. J., Nguyen, W. H., McGehee, M. D., Buonassisi, T. A 2-Terminal Perovskite/silicon Multijunction Solar Cell Enabled by a Silicon Tunnel Junction. *Appl. Phys. Lett.* **2015**, *106*, 121105.

(10) Albrecht, S., Saliba, M., Correa Baena, J. P., Lang, F., Kegelmann, L., Mews, M., Steier, L., Abate, A., Rappich, J., Korte, L., *et al.* Monolithic Perovskite/silicon-Heterojunction Tandem Solar Cells Processed at Low Temperature. *Energy Environ. Sci.* **2016**, *9*, 81–88.

(11) Werner, J., Barraud, L., Walter, A., Bräuninger, M., Sahli, F., Sacchetto, D., Tétreault, N., Paviet-Salomon, B., Moon, S.-J., Allebé, C., *et al.* Efficient Near-Infrared-Transparent Perovskite Solar Cells Enabling Direct Comparison of 4-Terminal and Monolithic Perovskite/Silicon Tandem Cells. *ACS Energy Lett.* **2016**, *1*, 474–480.

(12) Chen, B., Bai, Y., Yu, Z., Li, T., Zheng, X., Dong, Q., Shen, L., Boccard, M., Gruverman, A., Holman, Z., *et al.* Efficient Semitransparent Perovskite Solar Cells for 23.0%-Efficiency Perovskite/Silicon Four-Terminal Tandem Cells. *Adv. Energy Mater.* **2016**, *6*, 1–7.

(13) Fu, F., Feurer, T., Jäger, T., Avancini, E., Bissig, B., Yoon, S., Buecheler, S., Tiwari, A. N. Low-Temperature-Processed Efficient Semi-Transparent Planar Perovskite Solar Cells for Bifacial and Tandem Applications. *Nat. Commun.* **2015**, *6*, 8932.

(14) Kranz, L., Abate, A., Feurer, T., Fu, F., Avancini, E., Loeckinger, J., Reinhard, P., Zakeeruddin, S. M., Grätzel, M., Buecheler, S., *et al.* High-Efficiency Polycrystalline Thin Film Tandem Solar Cells. *J. Phys. Chem. Lett.* **2015**, *6*, 2676–2681.

(15) Bush, K. A., Palmstrom, A. F., Yu, Z. (Jason), Boccard, M., Cheacharoen, R., Mailoa, J. P., McMeekin, D. P., Hoye, R. L. Z., Bailie, C. D., Leijtens, T., *et al.* 23.6%-Efficient Monolithic Perovskite/Silicon Tandem Solar Cells with Improved Stability. *Nat. Energy*. **2017**, *2*, 17009.

(16) Duong, T., Mulmudi, H. K., Shen, H., Wu, Y., Barugkin, C., Mayon, Y. O., Nguyen, H. T., Macdonald, D., Peng, J., Lockrey, M., *et al.* Structural Engineering Using Rubidium Iodide as a Dopant under Excess Lead Iodide Conditions for High Efficiency and Stable Perovskites. *Nano Energy*. **2016**, *30*, 330–340.

(17) Yang, Z., Rajagopal, A., Jo, S. B., Chueh, C., Williams, S., Huang, C., Katahara, J. K., Hillhouse, H. W., Jen, A. K. Stabilized Wide Bandgap Perovskite Solar Cells by Tin Substitution. *Nano Lett.* **2016**, *16*, 7739–7747.

(18) Eperon, G. E., Leijtens, T., Bush, K. A., Prasanna, R., Green, T., Wang, J. T.-W., McMeekin, D. P., Volonakis, G., Milot, R. L., May, R., *et al.* Perovskite-Perovskite Tandem Photovoltaics with Optimized Band Gaps. *Science.* **2016**, *354*, 861–865.

(19) Noh, J. H., Im, S. H., Heo, J. H., Mandal, T. N., Seok, S. Il. Chemical Management for Colorful, Efficient, and Stable Inorganic-Organic Hybrid Nanostructured Solar Cells. *Nano Lett.* **2013**, *13*, 1764–1769.

(20) Unger, E. L., Kegelmann, L., Suchan, K., Sorell, D., Korte, L., Albrecht, S. Roadmap and Roadblocks for the Band Gap Tunability of Metal Halide Perovskites. *J. Mater. Chem. A*. **2017**, *5*, 11401–11409.

(21) Sutter-Fella, C. M., Li, Y., Amani, M., Ager, J. W., Toma, F. M., Yablonovitch, E., Sharp, I. D., Javey, A. High Photoluminescence Quantum Yield in Band Gap Tunable Bromide Containing Mixed Halide Perovskites. *Nano Lett.* **2016**, *16*, 800–806.

(22) Hoke, E. T., Slotcavage, D. J., Dohner, E. R., Bowring, A. R., Karunadasa, H. I., McGehee, M. D. Reversible Photo-Induced Trap Formation in Mixed-Halide Hybrid Perovskites for Photovoltaics. *Chem. Sci.* **2015**, *6*, 613–617.

(23) Eames, C., Frost, J. M., Barnes, P. R. F., O'Regan, B. C., Walsh, A., Islam, M. S. Ionic

Transport in Hybrid Lead Iodide Perovskite Solar Cells. *Nat. Commun.* **2015**, *6*, 7497.

(24) Yoon, S. J., Kuno, M., Kamat, P. V. Shift Happens. How Halide Ion Defects Influence Photoinduced Segregation in Mixed Halide Perovskites. *ACS Energy Lett.* **2017**, *2*, 1507–1514.

(25) Slotcavage, D. J., Karunadasa, H. I., McGehee, M. D. Light-Induced Phase Segregation in Halide-Perovskite Absorbers. *ACS Energy Lett.* **2016**, *1*, 1199–1205.

(26) Samu, G. F., Janaky, C., Kamat, P. V. A Victim of Halide Ion Segregation. How Light Soaking Affects Solar Cell Performance of Mixed Halide Lead Perovskites. *ACS Energy Lett.* **2017**, *2*, 1860–1861.

(27) Saliba, M., Matsui, T., Seo, J.-Y., Domanski, K., Correa-Baena, J.-P., Nazeeruddin, M. K., Zakeeruddin, S. M., Tress, W., Abate, A., Hagfeldt, A., *et al.* Cesium-Containing Triple Cation Perovskite Solar Cells: Improved Stability, Reproducibility and High Efficiency. *Energy Environ. Sci.* **2016**, *9*, 1989–1997.

(28) Saliba, M., Matsui, T., Domanski, K., Seo, J.-Y., Ummadisingu, A., Zakeeruddin, S. M., Correa-Baena, J.-P., Tress, W. R., Abate, A., Hagfeldt, A., *et al.* Incorporation of Rubidium Cations into Perovskite Solar Cells Improves Photovoltaic Performance. *Science.* **2016**, *354*, 206–209.

(29) Lee, J. W., Kim, D. H., Kim, H. S., Seo, S. W., Cho, S. M., Park, N. G. Formamidinium and Cesium Hybridization for Photo- and Moisture-Stable Perovskite Solar Cell. *Adv. Energy Mater.* **2015**, *5*, 1–9.

(30) Li, Z., Yang, M., Park, J. S., Wei, S. H., Berry, J. J., Zhu, K. Stabilizing Perovskite Structures by Tuning Tolerance Factor: Formation of Formamidinium and Cesium Lead Iodide Solid-State Alloys. *Chem. Mater.* **2016**, *28*, 284–292.

(31) Yi, C., Luo, J., Meloni, S., Boziki, A., Ashari-Astani, N., Grätzel, C., Zakeeruddin, S. M., Röthlisberger, U., Grätzel, M. Entropic Stabilization of Mixed A-Cation ABX 3 Metal Halide Perovskites for High Performance Perovskite Solar Cells. *Energy Environ. Sci.* **2016**, *9*, 656–662.

(32) McMeekin, D. P., Sadoughi, G., Rehman, W., Eperon, G. E., Saliba, M., Horantner, M. T., Haghighirad, A., Sakai, N., Korte, L., Rech, B., *et al.* A Mixed-Cation Lead Mixed-Halide Perovskite Absorber for Tandem Solar Cells. *Science.* **2016**, *351*, 151–155.

(33) Duong, T., Wu, Y., Shen, H., Peng, J., Fu, X., Jacobs, D., Wang, E., Kho, T. C., Fong, K. C., Stocks, M., *et al.* Rubidium Multication Perovskite with Optimized Bandgap for Perovskite-Silicon Tandem with over 26% Efficiency. *Adv. Energy Mater.* **2017**, *7*, 1–11.

(34) Beal, R. E., Slotcavage, D. J., Leijtens, T., Bowring, A. R., Belisle, R. A., Nguyen, W. H., Burkhard, G. F., Hoke, E. T., McGehee, M. D. Cesium Lead Halide Perovskites with Improved Stability for Tandem Solar Cells. *J. Phys. Chem. Lett.* **2016**, *7*, 746–751.

(35) Walsh, A. Principles of Chemical Bonding and Band Gap Engineering in Hybrid Organic–Inorganic Halide Perovskites. *J. Phys. Chem. C*. **2015**, *119*, 5755–5760.

(36) Amat, A., Mosconi, E., Ronca, E., Quarti, C., Umari, P., Nazeeruddin, M. K., Grätzel, M.,

De Angelis, F. Cation-Induced Band-Gap Tuning in Organohalide Perovskites: Interplay of Spin-Orbit Coupling and Octahedra Tilting. *Nano Lett.* **2014**, *14*, 3608–3616.

(37) Filip, M. R., Eperon, G. E., Snaith, H. J., Giustino, F. Steric Engineering of Metal-Halide Perovskites with Tunable Optical Band Gaps. *Nat. Commun.* **2014**, *5*, 1–9.

(38) Choi, H., Jeong, J., Kim, H., Kim, S., Walker, B., Kim, G., Young, J. Cesium-Doped Methylammonium Lead Iodide Perovskite Light Absorber for Hybrid Solar Cells. *Nano Energy*. **2014**, *7*, 80–85.

(39) Prasanna, R., Gold-parker, A., Leijtens, T., Conings, B., Babayigit, A. Band Gap Tuning via Lattice Contraction and Octahedral Tilting in Perovskite Materials for Photovoltaics. *J. Am. Chem. Soc.* **2017**, *139*, 11117–11124.

(40) Shao, Y., Yuan, Y., Huang, J. Correlation of Energy Disorder and Open-Circuit Voltage in Hybrid Perovskite Solar Cells. *Nat. Energy*. **2016**, *1*, 15001.

(41) Stolterfoht, M., Wolff, C. M., Amir, Y., Paulke, A., Perdigón-Toro, L., Caprioglio, P., Neher, D. Approaching the Fill Factor Shockley–Queisser Limit in Stable, Dopant-Free Triple Cation Perovskite Solar Cells. *Energy Environ. Sci.* **2017**, *10*, 1530–1539.

(42) Conings, B., Babayigit, A., Klug, M. T., Bai, S., Gauquelin, N., Sakai, N., Wang, J. T., Verbeeck, J., Boyen, H., Snaith, H. J. A Universal Deposition Protocol for Planar Heterojunction Solar Cells with High Efficiency Based on Hybrid Lead Halide Perovskite Families. *Adv. Mater.* **2016**, *28*, 10701–10709.

(43) Yang, W. S., Noh, J. H., Jeon, N. J., Kim, Y. C., Ryu, S., Seo, J., Seok, S. Il. High-Performance Photovoltaic Perovskite Layers Fabricated through Intramolecular Exchange. *Science.* **2015**, *348*, 1234–1237.

(44) Zheng, X., Chen, B., Dai, J., Fang, Y., Bai, Y., Lin, Y., Wei, H., Zeng, X. C., Huang, J. Defect Passivation in Hybrid Perovskite Solar Cells Using Quaternary Ammonium Halide Anions and Cations. *Nat. Energy*. **2017**, *2*, 17102.

(45) Wang, Z., Lin, Q., Chmiel, F. P., Sakai, N., Herz, L. M., Snaith, H. J. Efficient and Ambient-Air-Stable Solar Cells with 2D-3D Hetero-Structured Butylammonium-Caesium-Formamidinium Lead Halide Perovskites. *Nat. Energy*. **2017**, *2*, 17135.

(46) Jacobsson, J. T., Correa-Baena, J.-P., Pazoki, M., Saliba, M., Schenk, K., Gratzel, M., Hagfeldt, A. Exploration of the Compositional Space for Mixed Lead Halogen Perovskites for High Efficiency Solar Cells. *Energy Environ. Sci.* **2016**, *9*, 1706–1724.

(47) Rühle, S. The Detailed Balance Limit of Perovskite/silicon and perovskite/CdTe Tandem Solar Cells. *Phys. Status Solidi Appl. Mater. Sci.* **2017**, *214*, 1–10.

(48) Hörantner, M. T., Snaith, H. Predicting and Optimising the Energy Yield of Perovskite-on-Silicon Tandem Solar Cells under Real World Conditions. *Energy Environ. Sci.* **2017**, *10*, 1983–1993.

(49) Hörantner, M. T., Leijtens, T., Ziffer, M. E., Eperon, G. E., Christoforo, M. G., McGehee, M. D., Snaith, H. J. The Potential of Multijunction Perovskite Solar Cells. *ACS Energy Lett.* **2017**, *2*, 2506–2513.

(50) Rehman, W., Mcmeekin, D. P., Patel, J. B., Milot, R. L., Johnston, M. B., Snaith, H. J.,

Herz, L. M. Photovoltaic Mixed-Cation Lead Mixed-Halide Perovskites: Links between Crystallinity, Photo-Stability and Electronic Properties. *Energy Environ. Sci.* **2017**, *10*, 361–369.

(51) Hu, M., Bi, C., Yuan, Y., Bai, Y., Huang, J. Stabilized Wide Bandgap MAPbBrxI3–x Perovskite by Enhanced Grain Size and Improved Crystallinity. *Adv. Sci.* **2016**, *3*, 1500301.

(52) Zhou, Y., Wang, F., Cao, Y., Wang, J., Fang, H., Loi, M. A. Benzylamine-Treated Wide-Bandgap Perovskite with High Thermal-Photostability and Photovoltaic Performance. *Adv. Energy Mater.* **2017**, *7*, 1701048.

(53) Forgács, D., Pérez-del-Rey, D., Ávila, J., Momblona, C., Gil-Escrig, L., Dänekamp, B., Sessolo, M., Bolink, H. J. Efficient Wide Band Gap Double Cation – Double Halide Perovskite Solar Cells. *J. Mater. Chem. A*. **2017**, *5*, 3203–3207.